
Altimeter and velocity data fusion for enhanced spatiotemporal resolution of the Ice Sheet elevation

Peter Naylor

Φ-Lab, European Space Research Institute
European Space Agency
Frascati, 00044, Italy
peter.naylor@esa.int

Andreas Stokholm

DTU Space, Department of
Space Research and Space Technology
Technical University of Denmark
Kgs. Lyngby, 2800, Denmark
stokholm@space.dtu.dk

Abstract

Estimating changes in elevation of the ice sheets’ surface will provide a better understanding of the extent of melting ice sheets and their consequences. Satellite remote sensing, such as the CryoSat-2 radar altimeter satellite, is used to derive surface elevation. CryoSat-2 measures elevation data as point clouds across the Greenland ice sheet with large temporal and spatial gaps that approximately cover only 5% of the spatio-temporal domain of interest. The goal of this work is to fill the gaps in the domain of interest as accurately as possible. However, using only elevation data does not adequately link space and time, and hence, previous reconstruction attempts showed non-physical behaviour. To mitigate this, we propose to use velocity data, derived from Sentinel-1 Synthetic Aperture Radar (SAR) and interferometry (InSAR). Using both data products, with Physique Informed Neural Networks, enables a superior approach to fill the data gaps and link time and space appropriately; we call this a spatial-agreement term. We improve by 89% compared to a baseline, and the proposed spatial agreement term improves the performance by 11%.

1 Context

Global warming, accelerated in the polar regions, is causing substantial ice sheet loss, which drives global sea level rise and threatens ocean currents [5, 11]. Accurate elevation change measurements are an Essential Climate Variable vital for projects like the Ice Sheet Mass Balance Inter-comparison Exercise [2, 3]. Reliably determining ice loss is therefore paramount for informed political decision-making. Satellite altimetry, such as from the Ku-Band Synthetic Aperture Radar (SAR) CryoSat-2 (CS2) satellite, measures ice sheet elevation accurately. However, the CS2 altimeter data are unstructured point clouds with large spatiotemporal data gaps, complicating the creation of high-resolution grids [9]. Common interpolation methods can fail to capture long-term trends and reduce data resolution (rasterisation). We propose using deep learning to model these spatiotemporal changes.

Implicit neural representations (INR) can reconstruct surfaces from point clouds [8]. When constrained by physics, these become Physics-Informed Neural Networks (PINNs). We propose to apply PINNs for the reconstruction of the dynamic surface of the Greenland Ice Sheet (GrIS). The task is challenging, as the training data covers only 5.17% of the spatiotemporal area of interest. We propose to extend previous work aimed at reconstructing the GrIS with a single INR [7]. Instead, we couple the height information with velocity products derived from Sentinel-1 Synthetic Aperture Radar (SAR) [6] using interferometry (InSAR). To do this, we investigate training simultaneously two INR models, for height and for velocity, to improve the reconstruction error by allowing for cross-field regularisation. We apply our method to the Petermann glacier using 4 years of CS2 data.

Our contribution is the following. We conduct ablation studies on the proposed methods, using different model architectures, hyperparameters, and loss terms, with a focus on capturing temporal glacier dynamics. Reported results are evaluated on an independent data split and an alternative data source. We leave out random orbit acquisitions from CS2, and use Operation IceBridge (OIB) [15] laser altimeter data for broad spatiotemporal coverage. Finally, we compare our approach to an interpolation method and the best model trained on 12 decades of CS2 from a preceding study [7].

2 Method

2.1 Data

The altimeter data is acquired by CS2 data from the 1st of January 2017 till the 31st of December 2020 over the Petermann glacier in Northwest Greenland, spanning from the ocean to over 1,600 m in elevation, as illustrated in Fig. 1. The CS2 data is swath-processed according to Andersen et al. [1], providing several points in the swath across the orbit instead of a single point per swath. However, this approach requires phase unwrapping of the SAR altimeter data, which can result in elevation and location errors, appearing as sudden changes compared to surrounding measurements. The velocity products are derived from Sentinel-1 InSAR data, spanning the same period [13]¹. Petermann glacier is the second-largest floating ice tongue in Greenland and a major outlet glacier of the GrIS. It is a highly dynamic glacier, with seasonal variations in the ice velocity rates and the surface elevation change [13]. In addition to the CS2 orbits, the areas have been repeatedly measured by several airborne surface elevation campaigns, namely OIB [15]. The dataset comprises 37.4M CS2 points, where 10% of the daily acquired swaths are left for testing, and 20% of the remaining is used for validation. The OIB datasets consist of ten periods of sensing with 640K testing data points.

In order to reduce the errors and phase unwrapping errors in the CS2 data, we filter the CS2 points by creating local elevation averages, where we remove points which deviate by at least 3 times the standard deviation in the area. Finally, due to the far northern location of the Petermann Glacier, we project the data to the EPSG:3413 NorthStereo projection to not force the INR models to learn in addition a non-linear coordinate mapping.

Finally, we measure the performance of our model with 4 metrics: the Mean Absolute Error (MAE), the median error (MED), the mean error STandard Deviation (STD) and the daily standard deviation for the final gridded model output. The number of epochs is set to 60 epochs, the batch size is 8192, and AdamW is used. We perform hyperparameter selection (for the model width and depth, the learning rate, and all scalars in the loss) with 100 trials. We ensemble the five top-performing models on the validation set and report the standard deviation across the model performances. In addition, the reported daily standard deviation metric is defined as $T_{STD} = \mathbb{E}_t[\sqrt{\mathbb{V}_{x,y}(z)}]$. For this metric, a value of 0 implies a static solution, whereas a high value can imply non-physical dynamics.

2.2 Implicit Neural Representation

INR, i.e. coordinates-based NNs, are used for reconstructing spatially and temporally PCs [10], and map coordinates to a target value, h or v in this paper, called *a field*. This mapping function is estimated by fitting observations (t, u) , where t denotes the temporal component and u the spatial component, to the field of interest, an example is shown in Fig. 1. Desired properties are induced by application-based regularisation terms that can rely, like PINNs, on derivatives computed via backpropagation. Due to the intrinsic continuity and differentiability of NN, the interesting property of these models is their capability to interpolate the target field natively. Training an INR model involves optimising a loss function \mathcal{L} composed of multiple loss functions. One of these, a data-fitting term, pushes the INR to fit the training data, while the others regularise this estimated surface with a-priori knowledge of the physical properties of the surface. In addition to these, we regularise the INR with spatial gradients, $\mathcal{L}_S = \|\partial \cdot / \partial x\| + \|\partial \cdot / \partial y\|$ and temporal gradients, $\mathcal{L}_T = \|\partial \cdot / \partial t\|$. Hence, the loss function is defined as: $\mathcal{L} = \mathcal{L}_{data} + \lambda_S \cdot \mathcal{L}_S + \lambda_T \cdot \mathcal{L}_T$. Where λ_S and λ_T are fine-tuned scalars. The specific INR architectures used RFF [16] and SIREN [14].

¹As of today, the velocity product for other time periods has been released. Prior to 15/09/2025, only the years 2017 to 2021 were available.

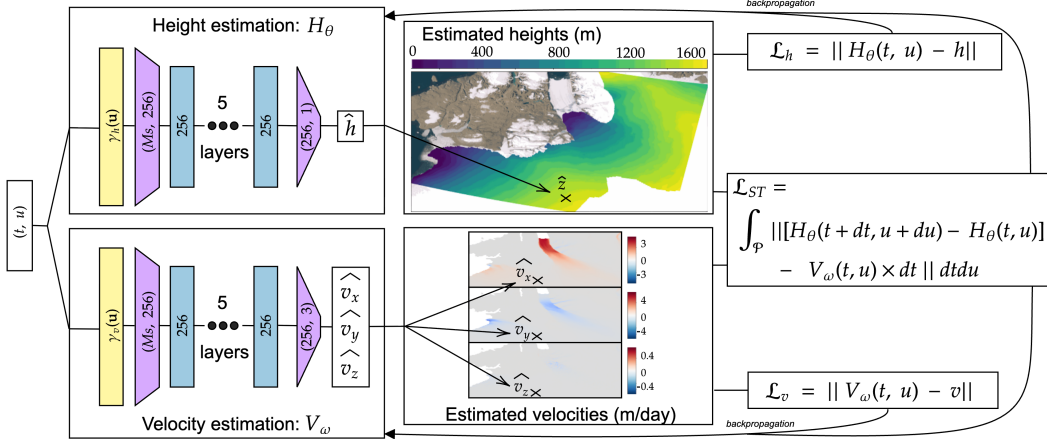


Figure 1: Method overview.

2.3 Proposed model

Inspired by another work [12], we propose a strategy aiming at reconstructing both the ice sheet elevation and the ice sheet velocity for the benefit of the elevation reconstruction, shown in Fig. 1. In particular, we use one INR for height reconstruction H_θ , which outputs one scalar, h , and one INR for velocity reconstruction V_ω , which outputs a velocity vector of size 3. This scheme allows us to integrate and link, in a differential manner, multiple aspects related to glaciology in Greenland. Specifically, this allows us to reconstruct both fields while allowing for interaction between the height and the velocity. The data fit term for H_θ is \mathcal{L}_H and V_ω is \mathcal{L}_V . Both sets of parameters are also penalised by a spatial-temporal agreement term named \mathcal{L}_{ST} . \mathcal{L}_{ST} is defined as the displacement of a point p_t given its velocity compared to the predicted position p_{t+1} . A graphical justification is provided in Fig. 2, and the loss is defined as: $\mathcal{L}_{ST} = \int_P ||[H_\theta(t + dt, u + du) - H_\theta(t, u)] - V_\omega(t, u) \times dt|| dt du$. Computationally speaking, at each iteration, we sample random spatiotemporal coordinates, given the estimations of the velocity, we compute du . We use du and H_θ to compute $\widehat{p_{t+1}}$ and then use the vertical velocity to compute $\widehat{p_{t+1}}$, which allows us to estimate the displacement error. Conceptualising this implies that the first derivative of the position should agree with the velocity. This formulation allows us to produce two INRs that are mutually intertwined, and due to the continuous nature of INR, allows us to retain the maximal temporal and spatial resolution of the original data. In addition, as the height and velocity fields are learned, in case of true disagreement, which could be due to a noisy acquisition or unwrapping error, or wrongly estimated velocities, the INR formulation allows for shifting one of the fields to better fit the overall loss. The final loss is: $\mathcal{L} = \mathcal{L}_H + \lambda_V \cdot \mathcal{L}_V + \lambda_{ST} \cdot \mathcal{L}_{ST} + \lambda_S \cdot \mathcal{L}_S + \lambda_T \cdot \mathcal{L}_T$. Where λ_T and λ_S are hyperparameters, whereas λ_V and λ_{ST} are dynamic and updated according to GradNorm [4] to better train the multi-objective loss. We name this option *Velocity (1)*, to differentiate from the model *Velocity (2)*, which does not use the vertical estimate velocity field and instead the temporal gradient of the height. This is motivated by the fact that the velocity products are superior at estimating horizontal displacement than vertical.

Another possible model could be a single INR with a spatial agreement term, but not on the estimated velocity product and instead using the actual velocity interpolated ground truth. This approach was quite computationally slower than the others and, therefore, discarded. Indeed, another advantage of having two INRs is that both produced estimations are directly on the GPU, allowing for skipping CPU-GPU transfer, increasing the computation time.

2.4 Baselines

To evaluate how the model performs, it is compared to a bilinear interpolation baseline and to the best-performing model from the previous study on Petermann [7]. For the bilinear interpolation, we compute the estimated height from an interpolation with all points within that month. ISRN is an INR using RFF with Random Orbit Sampling (ROS) trained on 12 years of CS2 data. ROS, compared to the Random Sampling (RS), does not split the training and validation set randomly but leaves out a

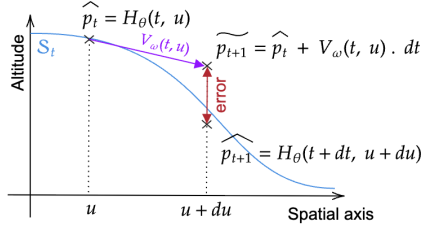


Figure 2: Deriving the physical penalty.

random orbit. This difference allows the model selection to maximise the temporal dynamic fit for the data by minimising the validation error based on random leave-out orbit acquisitions.

3 Results

In Table 1 we show the ablation results. We first notice that the spatiotemporal agreement term \mathcal{L}_{ST} helps reduce the daily standard deviation. It reduces the daily variation by one order of magnitude, as we can see from the differences in values of T_{STD} between the RS and Velocity options. On the test set of CS2, it is apparent that performance is only improved for SIREN. The best performing model on the CS2 test set is RFF with RS, but this model exhibits a high T_{STD} , implying a non-physical fit to the underlying data. The second-best performing model is SIREN with the velocity term and ISRIN Naylor et al. [7]. For the OIB datasets, we find that including the velocity term improves both performance compared to RS and ROS. On the OIB dataset, for SIREN, we see an improvement of 11% and 27% for RFF compared to a single INR with RS. This shows that the spatiotemporal agreement increases the model performance and links time and space scoring similarly to a model trained on 12 years of CS2 data rather than 4 years. Finally, the baseline approach, the bilinear interpolation, has a very low error, as the input and output values are identical. However, the error is much greater for data not seen before, such as the CS2 test set and OIB.

Table 1: Ablation study, comparison to baseline and previous state-of-the-art, best model is in bold and second best is underlined. The standard deviation is computed with 5 models.

| Datasets (\rightarrow) | | T_{STD} | CS2 | | | | | | OIB | | |
|---|--------------|------------------|-----------------|------------------|-----------------|-----------------|------------------|-----------------|-----------------|------------------|-----------------|
| (\downarrow) HP / Metrics (\rightarrow) | Option | | Train + Test | | | Test | | | MAE | MED | STD |
| RFF | RS | 1.58 ± 0.10 | 3.20 ± 0.07 | -0.11 ± 0.14 | 4.32 ± 0.06 | 3.19 ± 0.07 | -0.17 ± 0.13 | 4.42 ± 0.09 | 5.49 ± 0.15 | -0.09 ± 0.14 | 9.69 ± 0.21 |
| | ROS | 0.52 ± 0.02 | 3.52 ± 0.25 | -0.10 ± 0.23 | 4.77 ± 0.23 | 3.43 ± 0.27 | -0.13 ± 0.25 | 4.74 ± 0.26 | 4.81 ± 0.32 | -0.15 ± 0.38 | 8.83 ± 0.28 |
| | Velocity (1) | 0.06 ± 0.02 | 3.73 ± 0.05 | -0.27 ± 0.24 | 4.93 ± 0.04 | 3.63 ± 0.05 | -0.10 ± 0.22 | 4.96 ± 0.06 | 4.31 ± 0.10 | -0.00 ± 0.29 | 7.36 ± 0.10 |
| | Velocity (2) | 0.04 ± 0.05 | 4.03 ± 0.42 | -0.51 ± 0.55 | 5.15 ± 0.32 | 3.91 ± 0.39 | -0.34 ± 0.54 | 5.16 ± 0.30 | 4.64 ± 0.45 | -0.36 ± 0.71 | 7.61 ± 0.36 |
| SIREN | RS | 0.23 ± 0.35 | 3.43 ± 0.23 | 0.06 ± 0.32 | 4.74 ± 0.21 | 3.37 ± 0.22 | 0.14 ± 0.35 | 4.77 ± 0.22 | 4.13 ± 0.32 | 0.33 ± 0.40 | 7.78 ± 0.77 |
| | ROS | 0.32 ± 0.29 | 3.98 ± 0.82 | -0.78 ± 1.20 | 5.10 ± 0.60 | 3.88 ± 0.73 | -0.69 ± 1.12 | 5.14 ± 0.54 | 4.77 ± 1.07 | -0.71 ± 1.38 | 8.33 ± 0.97 |
| | Velocity (1) | 0.10 ± 0.11 | 3.25 ± 0.04 | -0.14 ± 0.10 | 4.64 ± 0.04 | 3.23 ± 0.04 | -0.07 ± 0.08 | 4.73 ± 0.05 | 3.71 ± 0.07 | 0.02 ± 0.41 | 7.48 ± 0.17 |
| | Velocity (2) | 0.01 ± 0.003 | 3.26 ± 0.06 | -0.23 ± 0.19 | 4.64 ± 0.05 | 3.23 ± 0.06 | -0.18 ± 0.19 | 4.71 ± 0.06 | 3.69 ± 0.11 | 0.15 ± 0.17 | 7.65 ± 0.17 |
| ISRIN [7] | | 0.29 ± 0.11 | 3.19 ± 0.09 | -0.35 ± 0.41 | 4.24 ± 0.14 | 3.23 ± 0.05 | -0.31 ± 0.47 | 4.26 ± 0.13 | 3.67 ± 0.12 | -0.07 ± 0.15 | 6.63 ± 0.12 |
| Bilinear interpolation | | X | 1.90 | 0.00 | 13.42 | 12.41 | 0.00 | 34.16 | 6.99 | -0.023 | 14.06 |

4 Conclusion

We proposed a novel methodology for reconstructing the GrIS elevation that combines two INRs, one used for height estimation and a second for estimating the velocity. These INRs are combined via an additional spatiotemporal agreement term in the loss. This loss term allows for correctly linking the temporal to the spatial dynamics compared to previous methods relying on different validation schemes. The proposed approach achieved the best performance on the CS2 test set and OIB when restricted to the same available training dataset, compared to the baseline and previous approaches. Our proposed approach (SIREN with velocity (2)) outperforms the bilinear interpolation by a large margin, 89% lower MAE on OIB, and exhibits similar performances and temporal dynamics to previous work on the CS2 test set. In addition, our method, like previous work, produces physically plausible estimations of the GrIS elevation. Our proposed approach is more data-driven and naturally produces height estimation and velocity estimation for any point in space and time. Future work involves: *i*) Scaling up this proof-of-concept temporally to include all available velocity products from 2014 to 2023. *ii*) Validating the resulting reconstruction velocity product. *iii*) Extending the geographical area of interest from the Petermann Glacier to the whole of Greenland Ice Sheet.

Acknowledgement

The authors acknowledge the use of the SpaceHPC high-performance computing facility in ESRIN for the model parameter optimisation conducted in this research.

References

- [1] Natalia Havelund Andersen, Sebastian Bjerregaard Simonsen, Mai Winstrup, Johan Nilsson, and Louise Sandberg Sørensen. Regional Assessments of Surface Ice Elevations from Swath-Processed CryoSat-2 SARIn Data. *Remote Sensing*, 13(11):2213, jun 5 2021.
- [2] Andrew Shepherd, Erik Ivins, et al. Mass balance of the antarctic ice sheet from 1992 to 2017. *Nature* 558, 219–342 222, 2018.
- [3] Aqsa Patel, et al. Fine-resolution radar altimeter measurements on land and sea ice. *IEEE Transactions on Geoscience and Remote Sensing*, Vol. 53, No. 5, 2015.
- [4] Zhao Chen, Vijay Badrinarayanan, Chen-Yu Lee, and Andrew Rabinovich. Gradnorm: Gradient normalization for adaptive loss balancing in deep multitask networks. In *International conference on machine learning*, pages 794–803. PMLR, 2018.
- [5] Peter Ditlevsen and Susanne Ditlevsen. Warning of a forthcoming collapse of the Atlantic meridional overturning circulation. *Nature Communications*, 14(1), jul 25 2023. [Online; accessed 2024-08-06].
- [6] Thomas Nagler, Helmut Rott, Markus Hetzenegger, Jan Wuite, and Pierre Potin. The Sentinel-1 mission: New opportunities for ice sheet observations. *Remote Sensing*, 7(7):9371–9389, 2015. doi: 10.3390/rs70709371. URL <https://www.mdpi.com/2072-4292/7/7/9371>.
- [7] P. Naylor, A. Stokholm, N. Dionelis, N. H. Andersen, Q. Paletta, and S. B. Simonsen. Implicit neural representation for ice sheet surface elevation reconstruction to assess elevation change in high-spatiotemporal resolution. Preprint, 2025. URL <https://ssrn.com/abstract=5447938>.
- [8] Peter Naylor, Diego Di Carlo, Arianna Traviglia, Makoto Yamada, and Marco Fiorucci. Implicit neural representation for change detection. In *Proceedings of the IEEE/CVF Winter Conference on Applications of Computer Vision*, pages 935–945, 2024.
- [9] Johan Nilsson and Alex S. Gardner. Elevation Change of the Greenland Ice Sheet and its Peripheral Glaciers: 1992–2023. [preprint], in review, 2024. *The Cryosphere*, oct 21 2024. [Online; accessed 2025-02-28].
- [10] Maziar Raissi, Paris Perdikaris, and George E Karniadakis. Physics-informed neural networks: A deep learning framework for solving forward and inverse problems involving nonlinear partial differential equations. *Journal of Computational physics*, 378:686–707, 2019.
- [11] Mika Rantanen, Alexey Yu. Karpechko, Antti Lipponen, Kalle Nordling, Otto Hyvärinen, Kimmo Ruosteenoja, Timo Vihma, and Ari Laaksonen. The Arctic has warmed nearly four times faster than the globe since 1979. *Communications Earth & Environment*, 3(1), aug 11 2022. [Online; accessed 2024-08-06].
- [12] Lu Sang, Zehranaz Canfes, Dongliang Cao, Florian Bernard, and Daniel Cremers. Implicit neural surface deformation with explicit velocity fields. *arXiv preprint arXiv:2501.14038*, 2025.
- [13] Copernicus Climate Change Service. Greenland ice sheet annual gridded velocity data from 2017 to present derived from satellite observation, 2020. URL <https://cds.climate.copernicus.eu/>. Accessed on 25-02-2025.
- [14] Vincent Sitzmann, Julien Martel, Alexander Bergman, David Lindell, and Gordon Wetzstein. Implicit neural representations with periodic activation functions. *Advances in neural information processing systems*, 33:7462–7473, 2020.
- [15] M Studinger. Icebridge ATM L2 Icessn Elevation, Slope, and Roughness, Version 2. [ILATM2.002] (<https://nsidc.org/icebridge/portal/map>).

- [16] Matthew Tancik, Pratul Srinivasan, Ben Mildenhall, Sara Fridovich-Keil, Nithin Raghavan, Utkarsh Singhal, Ravi Ramamoorthi, Jonathan Barron, and Ren Ng. Fourier features let networks learn high frequency functions in low dimensional domains. *Advances in neural information processing systems*, 33:7537–7547, 2020.